Acta Materialia 206 (2021) 116599

Contents lists available at ScienceDirect

Acta Materialia

journal homepage: www.elsevier.com/locate/actamat

Initiation of fatigue damage in ultrafine grained metal films

O. Glushko*, D. Kiener

Chair of Materials Physics, Department Materials Science, Montanuniversität Leoben, Jahnstr. 12, 8700 Leoben, Austria

ARTICLE INFO

Article history:
Received 21 August 2020
Revised 27 November 2020
Accepted 19 December 2020
Available online 27 December 2020

Keywords:
Fatigue
Damage initiation
Ultrafine grained
Microstructure
Thin films

ABSTRACT

The aim of the current research work is to understand how individual local microstructure features such as grain size, grain orientation, grain boundary characteristics, as well as the global parameters of the microstructure (texture, grain size distribution, twin boundary fraction) influence the process of fatigue damage initiation in thin films. Cyclic strain with an amplitude of 1% was applied to polymer-supported ultrafine grained gold and copper films allowing for observation of numerous independent localized plasticity events within a single macrosample. Detailed electron backscatter diffraction analysis of the microstructure in the vicinity of these plasticity events was performed to gain statistical information and elucidate robust correlations. On the local scale, the damage was initiated in large grains (>1 μm) in the vicinity of coherent twin boundaries specifically oriented with respect to the loading direction. When appropriate large grains were not present in the initial microstructure, mechanically induced grain coarsening preceded fatigue damage initiation. If the initial microstructure did not contain properly oriented coherent twin boundaries, then the local grain size of dynamically coarsened grains was the sole parameter controlling plastic slip localization. On the global scale, the major parameters of the microstructure influencing the fatigue damage initiation process are the fraction of twin boundaries, texture, and the width of the grain size distribution. Based on the presented results a clear strategy for improving the fatigue life of thin films is proposed.

1. Introduction

Fatigue damage initiation in single-crystalline metals is well understood. Cyclically applied mechanical load leads to generation, movement, and multiplication of dislocations. After a certain number of loading cycles, dislocations start to agglomerate and form so-called persistent slip bands (PSBs) which act as zones of cyclic strain localization [1–5]. The application of further loading cycles results in development of extrusions, intrusion, and cracks within the PSBs. This classical mechanistic picture is formulated without taking into account the existence of grain boundaries (GBs), but it still works well for polycrystalline materials as long as the grain size is significantly larger than the characteristic length scale of the dislocation wall structures within a PSB, which is on the order of 1 μm. With decreasing grain size the GBs start to affect the fatigue damage initiation process. On the one hand, GBs are obstacles for dislocation motion, thus the size of a PSB is restricted by the size of the related grain. On the other hand, specific GBs can act as strain localization sites and thus compete with strain localization due to PSB formation. For instance, it was shown that in steel samples with grain sizes of several tens of micrometers the cracks can be initiated both from PSBs and GBs [6–9]. A particularly specific GB which was frequently reported to act as a crack initiation site is the coherent twin boundary (CTB) [10–15]. The classical model by Heinz and Neumann [12] suggests that strain localization near a CTB occurs due to the mismatch of elastic modulus between parent and twin. Systematic research work on fatigue crack initiation in precipitate strengthened fcc Ni-based superalloys with average grain sizes of about 30 μm demonstrated that fatigue cracks were always initiated close to a CTB [13–15]. When a material becomes ultra-fine grained (i.e. with grain sizes between 100 nm and 1 μm), the dislocations induced by cyclic mechanical load are unable to travel for distances long enough to form classical PSBs. Instead, local slip bands and extrusions within single grains are observed, or the cracks are initiated directly on GBs [16]. It is thus to expect that specific grain orientations and GBs with specific properties will act as weak links responsible for fatigue crack initiation in an UFG material.

Numerous research works have reported about the evolution of fatigue damage in free-standing UFG and nanocrystalline samples [17–26], however, without placing much emphasis on the damage initiation with respect to the material microstructure. These works focused rather on fatigue crack propagation [20,21,23,24] or

* Corresponding author.
E-mail address: oleksandr.glushko@unileoben.ac.at (O. Glushko).

https://doi.org/10.1016/j.actamat.2020.116599

on general fatigue life measurements for comparison with the large database of bulk materials [17,19,21,22]. Although the initiation of fatigue cracks was addressed in detail in [23], pre-notched samples were employed in this study so the cracks were always observed at the notch tip. A more promising strategy to access the early stage of fatigue damage is to deposit a film on a substrate with high elastic limit and apply global cyclic strain so that the substrate deforms elastically, but the film accumulates plastic strain. The advantage of such a test design is that the substrate prevents global strain localization and numerous independent events of fatigue damage formation and propagation can be observed for a single sample, thereby largely removing stochastic or singular effects. A polymer-supported film seems to be the perfect model system for the investigation of fatigue damage initiation, since in the absence of global defects only the intrinsic film microstructure will control where and when the damage forms. Notably, the main drawback of this approach is the inability to simultaneously measure the fatigue life to compare to bulk samples.

A series of research works was published by the group of O. Kraft considering Cu, Al, and Au films [16,27–30] on polymer substrates subjected to cyclic strain, with the main focus on cyclic stress-strain behavior, damage morphology and in-depth transmission electron microscopy (TEM) characterization of dislocation activity. It was shown that fatigue cracks start to grow from extrusions in thicker films, while in thinner ones they nucleate and grow at grain boundaries. Regarding the initiation of fatigue damage, it was only stated that the extrusions "occur in the larger grains of all the films" [16]. In a recent study [31], fatigue behavior of nanocrystalline gold films with different thicknesses on polyimide substrates was analyzed in detail by scanning electron microscopy (SEM) and TEM. The importance of dynamic grain coarsening for fatigue damage initiation and propagation was clearly demonstrated, but possible correlations between the damage initiation sites with respect to the local microstructure were not investigated. Other reports on fatigue in polymer-supported metal films [32–39] have also not considered the early stage of strain localization, but were focused rather on thickness-dependent fatigue life, crack propagation and crack morphology, as well as electrical conductivity degradation.

To sum up the state of the art regarding the early stage of fatigue damage initiation, a number of works have reported that in fine-grained materials (grain size from 1 to 100 μm), cyclic strain typically localizes close to a CTB [6,7,13–15] and the grain size and local Schmid factor act as additional factors [13–15]. Further, in UFG and nanocrystalline materials the fatigue damage initiation sites were found with higher probability within larger grains [16]. Moreover, local grain coarsening was frequently observed to occur simultaneously with local plasticity or crack propagation [19–21,26,31].

In this work polymer-supported Au and Cu films with tailored distinctly different microstructures are employed in an attempt to uncover the local and global parameters of the material microstructure responsible for the localization of plastic strain at the early stage of fatigue damage in UFG films.

2. General background remarks

The approach to access fatigue damage initiation mechanisms used in this work is fairly straightforward. A given amount of straining cycles is applied to a polymer-supported film with particular microstructure in order to induce cyclic damage. Ideally, the strain amplitude and cycle number should be adjusted in a way that pronounced but rather localized plastic deformation events can be observed on the film surface under the condition that no visible defects or stress concentration points are in the vicinity. Then the microstructures of the areas surrounding the local plastic deformations are examined using electron backscatter diffraction (EBSD). Finally, it is expected that by analyzing dozens of local plastic deformation events it will be possible to identify global and/or local parameters of the microstructure (i.e. parameters of grains and GBs) common for all fatigue damage initiation sites with high statistical significance.

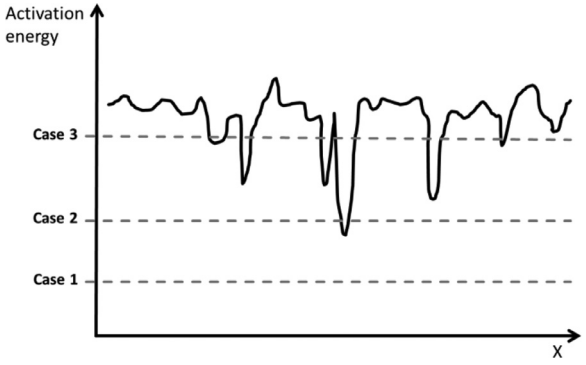

Fig. 1. Hypothetic energy landscape for activation of cyclic plastic deformation. Particular microstructural features (grains with specific orientation and/or size, vicinity of GBs with specific properties, grains with higher density of dislocation sources) possess lower activation energy for localization of plastic strain. Three distinct cases are possible depending on the amplitude of applied stress: no plasticity is induced (Case 1), only the deepest minima are activated (Case 2), or numerous fatigue damage initiation sites are activated simultaneously (Case 3).

To visualize this train of thought, let us assume exact knowledge of the stress required to activate cyclic plasticity in each point of the microstructure. If one would regard an imaginary profile over the sample surface, then an activation energy landscape can be built. At some points the activation energy is high, in others lower, and there will be local and global minima, as shown schematically in Fig. 1. By adjusting the applied strain amplitude one can tailor how many local minima will be activated. In the case that the applied cyclic mechanical load is too low (Case 1), the material remains purely elastic and no plastic strain localization is observed. Case 2 corresponds to the situation when only the deepest minima are activated, leading to low density of the damage initiation sites while most of the film will remain in the elastic regime. In Case 3 many different local minima will be activated, thus a high density of plastic localization and damage initiation will be observed. The activation energy landscape depends strongly on the material and respective microstructure. For instance, by decreasing the grain size one can significantly shift the whole activation energy landscape to higher energies even for the same material and texture. In this work, we explore different materials and microstructures using the same strain amplitude – 1%, so that the polyimide substrate stays in purely elastic regime but significant plastic deformation can be accumulated within the film with increasing cycle number. Depending on the film microstructure, this strain amplitude can correspond to different cases for the respective energy landscapes, leading to high or low area density of initiation sites.

The concept presented in Fig. 1 is simplified, since it assumes that the landscape does not change during cyclic loading, which is not necessarily the case. Although an evolution of the activation energy landscape with the cycle number might lead to disappearance of some minima and appearance of new minima, we hypothesize that the local microstructure, i.e. grain size and orientation as well as GB parameters, predominantly determine the damage initiation process. With the help of the activation energy landscape concept, we postulate that there are "weak links" which are prone to the plastic strain localization, and current research work is intended to establish whether there is a clear correlation between

Table 1
Overview of investigated sample types and their initial microstructures.

N	Material, thickness	Deposition method	Grain size	Texture (for more details see supplementary Fig. S1)	Fraction of Twin Boundaries
1	Au, 250 nm	evaporation	145±40 nm	strong: 92%@(111)	~10%
2	Au, 500 nm	evaporation	210±60 nm	strong:89%@(111)	~12%
3	Cu, 250 nm	evaporation	bi-modal	moderate: 60%@(111), 20%@(511)	N/A
4	Cu 500 nm	sputtering (in 8 cycles)	270±90 nm	weak: 36% (111), 16%@(511)	~25%
5	Cu 500 nm	sputtering	730±220 nm	no texture	~60%

the local microstructure parameters accessible with EBSD and the activation energy minima – those "weak links" where localization of plastic deformation will be observed at first.

3. Experimental

Aiming at studying UFG thin films with distinctly different microstructures, here we consider five thin film systems with microstructures described in Table 1. Au films with thicknesses of 250 nm and 500 nm were deposited by electron beam evaporation on 125 µm polyimide (Upilex S) substrates. The deposition was performed at room temperature in a Balzers BAK 550 evaporation machine with a vacuum of 2.1×10^{-5} Pa and using a deposition rate of 0.3 nm/s. A 10 nm thick Cr layer was deposited prior to the gold film to improve adhesion. No annealing or any other post-treatment procedures were applied to the films. The 250 nm thick Cu films were deposited using similar parameters on the same evaporation system.

Furthermore, two sputter deposited Cu films with a thickness of 500 nm are considered in this work. In one case the films were deposited in an FHR Line 600V modular inline sputter system. The substrates were fixed onto the carrier in the load-lock chamber and after reaching a base pressure of 1×10^{-4} Pa, plasma etching of the polyimide substrates was performed. The Cu films were deposited in 8 cycles (approximately 63 nm per cycle) to obtain an ultra-fine grained microstructure. The second 500 nm thick Cu film was deposited in a custom-built laboratory-scale sputtering system based on unbalanced AJA A320 XP magnetrons with a base pressure $< 10^{-4}$ Pa. The whole film was deposited in one cycle on the plasma-etched polyimide substrate.

The test samples with width of 4 mm and length of 40 mm were cut using a scalpel from larger sheets. Mechanical testing was performed on an MTS Tytron 250 tensile testing device using a gage length of 20 mm. Cyclic loading was applied in strain control mode by means of a sine strain function oscillating between the initial position (zero strain) and the peak value of 1% with a frequency of 0.5 Hz. The number of cycles leading to the appearance of local plasticity events but still prior to crack propagation was determined experimentally for each thin film system by microscopic inspection. It is important to mention that fatigue experiments on polymer-supported films are different from the classical Coffin-Manson low cycle fatigue experiments [40]. Due to the polymer support, there is no total sample fracture and the number of cycles to failure cannot be unambiguously defined. Additionally, since the polymer substrate is much thicker than the film, the total applied force is carried mostly by the substrate and the film stress cannot be acquired directly from the applied loading/straining profile. The current experimental design is intended to achieve the main aim of the study – capturing the early stage of fatigue damage initiation and establishing statistically robust correlations with respect to the microstructure. The evaluation of materials fatigue life for comparison with bulk or micromechanical samples is out of scope of this work; interested readers are referred to Refs. [27–30].

Scanning electron microscopy characterization was performed using a Zeiss Leo 1525 at an acceleration voltage of 5 kV and with a 30 µm aperture. All micrographs shown below were taken using the in-lens detector. EBSD characterization was performed with an acceleration voltage of 20 kV and step sizes between 30 and 60 nm, depending on the film microstructure. For each thin film system at least 30 damage initiation sites were detailed by EBSD for the analysis of crystal orientation correlations. The fraction of TBs was deduced using the corresponding identification routine of the Orientation Imaging Microscopy software (OIM Analysis™ 5.31), which is based on orientation relations. Tolerance angle of 5° was assumed during the identification of TBs. Since the inclination of the GB planes with respect to the surface is generally unknown, both coherent and incoherent TBs are included. For texture quantifications the (111) ND and (511) ND directions with tolerance misorientation of 10° were chosen. The corresponding areas of grain orientations on an inverse pole figure are depicted in supplementary figure Fig. S1. The (511) ND orientation corresponds to the twin component of (111) ND oriented grains as demonstrated in supplementary figure Fig. S2.

4. Results

4.1. Crack initiation in textured gold films

The initial microstructures of thermally evaporated gold films with thicknesses of 250 nm and 500 nm are shown in Fig. 2. Both films exhibit strong (111) fiber texture but slightly different microstructures. The 250 nm films possess lower average grain size of 145±40 nm and narrower grain size distribution in comparison to the 500 nm thick films having grain sizes of 210±60 nm and a distribution with a larger "tail" approaching 1 µm (Fig. 2d). Both films exhibit low fractions of TBs – between 10% and 15%.

Successive development of fatigue damage with increasing cycle number is demonstrated in Fig. 3 for the 250 nm thick Au films. The cracks are always initiated within the areas of extended local plasticity, as shown in Fig. 3a and b. These local plasticity areas appearing bright in the SEM images (in contrast to the dark grey pristine surface) correspond to single grains which have dynamically grown during cyclic loading. The mechanisms of room temperature grain coarsening induced by cyclic strain were discussed in great details in a recent paper [41]. After initiating inside the coarsened grains, the cracks start to propagate with increasing cycle number as shown in Fig. 3c and d. The density and length of cracks also increases with cycle number (Fig. 3e and f) and are expected to reach saturation after applying a high enough cycle number as predicted by the shear lag model [42,43].

Detailed characterization of the microstructure of a typical crack initiation site is given in Fig. 4. The SEM image and corresponding grain orientation map in ND direction are provided in Fig. 4a and b, respectively. As one can see, the extrusion/crack couple is located inside a heavily coarsened grain with a size of about 5 µm, i.e. more than an order of magnitude larger than the average grain size of the initial microstructure. This grain has no specific orientation which would explain extended local plasticity, since it exhibits neither a high maximum Schmid factor (Fig. 4c) nor a low Taylor factor (Fig. 4d). Orientations of 20 randomly chosen grains where local plasticity was observed are depicted in an inverse pole

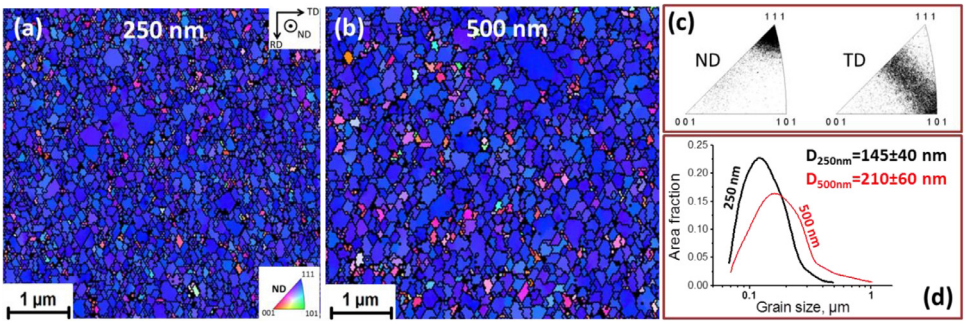

Fig. 2. Initial microstructure of thermally evaporated gold films. The grain orientation maps for 250 nm and 500 nm thick films are shown in (a) and (b), respectively. The inverse pole figures for both film thicknesses are given in (c). The grain size distributions and average grain sizes are depicted in (d).

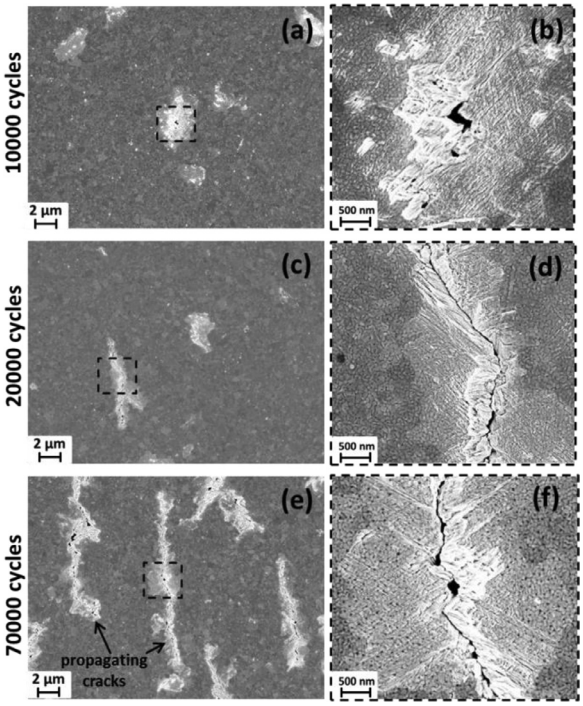

Fig. 3. SEM images showing the development of fatigue damage in 250 nm thick Au films after 10000 (a, b), 20000 (c, d) and 70000 (e, f) cycles with 1% peak strain. Images (b, d, f) are enlarged portions from the dashed squares in (a, c, e), respectively. The straining direction is horizontal.

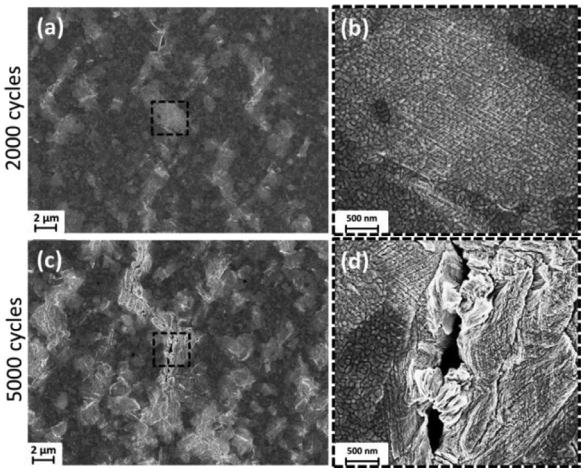

Fig. 5. SEM images detailing the morphology of fatigue damage in 500 nm thick Au films after 2000 cycles (a, b) and 5000 cycles (c, d). Images (b) and (d) present enlarged portions from the dashed rectangles in (a) and (c), respectively. The straining direction is horizontal.

figure (IPF) shown in supplementary Fig. S3 to further confirm that no specific grain orientation can be associated with plastic slip localization. It can be concluded that the size of this dynamically coarsened grain is the sole reason for the localization of plastic slip and crack initiation. According to the Hall-Petch relationship [44,45] larger grains have lower yield stress, thereby promoting local plastic slip and accumulation of damage within these grains.

In principle the same fatigue damage initiation mechanism holds also for the 500 nm thick Au films. Notably, the grains coarsen much faster with cycle number and crack initiation occurs significantly earlier, already after 2000 cycles as shown in Fig. 5. Cyclic plasticity localizes within dynamically coarsened grains in form of numerous surface slip steps (Fig. 5b) which then develop to cracks with increasing number of applied cycles (Fig. 5d). One can also see that in 500 nm thick films a significantly higher surface fraction is plastically deformed in comparison to the 250 nm thick films, where the major fraction of the surface remains

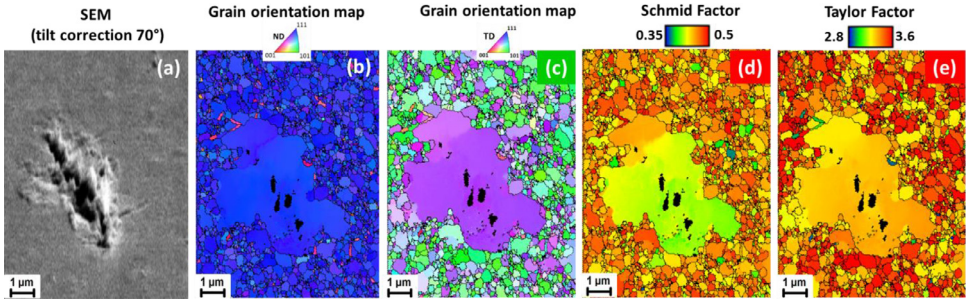

Fig. 4. Analysis of a typical crack initiation site in 250 nm thick Au films, showing an SEM image (a), the EBSD grain orientation map normal to the surface (b), the EBSD grain orientation map in the straining direction (s), Schmid factor map (d), and Taylor factor map (e), respectively. The straining direction is horizontal.

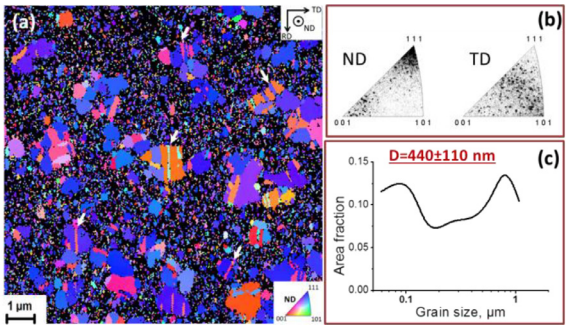

Fig. 6. Initial microstructure of bimodal 250 nm thick Cu films. The EBSD grain orientation map is shown in (a), the corresponding inverse pole figures in (b), and the related grain size distribution in (c). The straining direction is horizontal (TD). Black color in (a) depicts areas which were not indexed by EBSD, corresponding to the nanocrystalline parts of the microstructure. White arrows in (a) highlight some examples of TBs inside large grains.

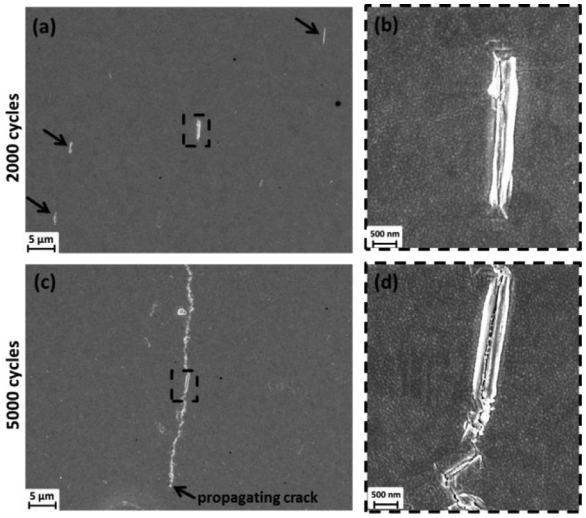

Fig. 7. SEM images of typical crack initiation sites in a 250 nm thick copper film with bimodal grain size distribution. After 2000 cycles no cracks but localized extrusions marked by arrows in (a) are seen. Enlarged portion of (a) showing such localized extrusion is given in (b). After 5000 cycles propagation of cracks (c) initiated at the localized extrusions detailed in (d) is observed. The straining direction is horizontal.

damage-free (Fig. 3). This difference can be caused either by the film thickness or by the difference in the initial grain size distribution. As seen from Fig. 2d, 250 nm thick films have virtually no grains above 400 nm in size. In contrast, the 500 nm thick films contain a noticeable fraction of grains with sizes up to 1 μm. Since it is difficult to fabricate films with different thicknesses but exactly the same microstructure, a series of annealing treatments of 250 nm thick films was performed in order to induce a slight grain coarsening prior to mechanical test. After gentle annealing for 2 hours at 75°C, the average grain size of the 250 nm thick Au films grew to 240±70 nm with some grains up to 1 μm in size, which very similar to the grain size distribution of as-deposited 500 nm thick films. The annealing treatment did not lead to any noticeable changes in the fatigue damage initiation process in 250 nm thick films. Swifter grain coarsening with cycle number and, as a consequence, much faster initiation of surface damage in 500 nm thick is thus attributed to the difference in film thickness. A potential explanation of this effect is based on experimental observations suggesting that grain boundary migration occurs through the movement of grain boundary steps, also called disconnections [46,47]. Generation of new disconnections can occur through the absorption of lattice dislocations by the grain boundary. Due to the larger height more lattice dislocations can impinge the grain boundary in 500 nm thick films in comparison to 250 nm thick films, thereby providing more steps for grain boundary migration. Additionally, thicker grains have larger dislocation sources leading to lower stress required for the generation of new dislocations.

4.2. Crack initiation in copper films with bimodal grain size distribution

In Fig. 6 the initial microstructure of 250 nm thick thermally evaporated Cu films is presented. They have a bimodal grain size distribution with peaks at about 1 μm and below 100 nm (Fig. 6b). It is important to note that proper detection of grains smaller than 60 nm in size using EBSD technique is difficult, since the Kikuchi patterns are formed by electrons that penetrated to depths of 20-30 nm in the material. Therefore, there are only few unambiguously indexed pixels per grain, which is not enough to determine the grain size. As a result, approximately 35% of the surface area cannot be properly indexed and appears black in (a). Additional examination using the backscatter electron detector (see supplementary material, Fig. S5) confirmed the existence of a nanocrystalline matrix between the large grains. Due to the significant fraction of non-indexed points, it is difficult to identify the fraction of TBs unambiguously. However, it can be recognized in Fig. 6a that most of the large grains contain TBs, with some exemplarily indicated by white arrows. As seen in Fig. 6b, the texture of the films is also bimodal with about 60% close to (111) ND component and a weaker component of about 20% close to (511) ND, which corresponds to the twin component of the (111) oriented grains.

Crack initiation sites can be clearly observed in these films after applying 2000 cycles with 1% strain. As depicted in Fig. 7a and b, sparsely distributed strongly localized plastic deformations in the form of extrusions are induced, while the rest of the surface remains unchanged. After 5000 cycles numerous cracks propagating from the crack initiation sites are observed on the surface, an example of which is shown in Fig. 7c. The enlarged image (Fig. 7d) demonstrates that the crack indeed started from a localized extrusion.

The SEM micrograph of a typical crack initiation site as well as the corresponding EBSD grain orientation map are shown in Fig. 8a and b, respectively. To make the correlation between SEM image and grain orientation map more evident, white triangles mark identical positions in both images. The localized extrusion is formed in the vicinity of CTB inclusions in a grain with an orientation close to (100) ND. The size of the parent grain is about 3 μm in equivalent diameter. With the help of more detailed orientation analysis of different parent-twin pairs associated with the localization of plastic strain presented in Fig. 8c and d (parameters of all analyzed pairs are listed in the supplementary Table S1), several clear trends can be detected. As follows from Fig. 8c, all parent grains are oriented close to (100) ND direction within a tolerance angle of about 10°. Even though in the straining direction (Fig. 8d) the considered parent-twin pairs seem to be distributed rather randomly, three different groups can be clearly detected. In the first group both parent and twin have maximum Schmid factors of 0.48 or more. Due to the high resolved shear stress accumulation of plastic slip in such grains occurs quickly with increasing number of applied cycles. The second group involves grains with a “stiff” twin inclusion having an elastic modulus 1.5 to 1.8 times higher than the parent in straining direction. This case corresponds to the model of Heinz and Neumann [12], which explains appearance of high local strains by the elastic mismatch in elastically anisotropic materials. The third group contains pairs with the same maximum Schmid factor that corresponds to the parallel slip configuration, i.e. when the CTB plane is parallel to the slip

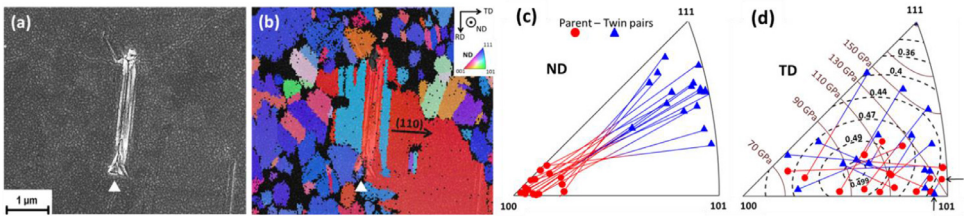

Fig. 8. Microstructural analysis of fatigue damage initiation sites in 250 nm thick Cu films with bi-modal grain size distribution. A typical crack initiation site is demonstrated by an SEM image (a) and corresponding EBSD grain orientation map (b). Inverse pole figures showing orientations of parent and twin grains associated with the localized extrusions in the surface normal direction and straining direction are depicted in (c) and (d), respectively. In (d) additional contours of the equal maximum Schmid factor (dashed black) and elastic modulus (solid brown) are included. The white triangles mark the identical position in (a) and (b). Two black arrows in (d) indicate a pair with rather low maximum Schmid factor and parallel slip configuration. The straining direction is horizontal.

plane [13]. An example of such a pair is depicted in Fig. 8d by two black arrows. In parallel slip configuration, activated dislocations can easily travel without crossing a grain boundary, which leads to fast accumulation of plastic strain, as was demonstrated by direct measurements using digital image correlation [13].

It is important to mention that in the initial bi-modal microstructure numerous large grains are present and most of them contain twin boundaries, as exemplarily indicated by white arrows in Fig. 6a. Additional analysis of the orientations of large grains with twin inclusions in the initial microstructure, as shown in Supplementary Fig. S6, proves that the texture of large twinned grains resembles the general texture with the major component close to (111) ND (Fig 6b). However, only large grains with twin inclusions *and* orientations close to (100) ND act as crack initiation sites. The parent grains that initiated damage were larger than the largest grains in the initial microstructure, indicating that dynamic grain coarsening has supported plastic slip localization also in this case, although the existence of sparsely distributed large grain outliers cannot be completely ruled out. Additionally, local grain coarsening was observed in the wake of propagating cracks and in front of the crack tips. We regard grain coarsening as an important prerequisite for crack propagation, as it softens the material locally, thus enhancing accumulation of cyclic plastic strain.

Provided analysis allows formulation of the following three main correlations between the damage initiation and microstructure: (i) crack initiation sites are always next to a CTB, (ii) the orientation of parent grains are always close to (100) ND, (iii) the parent grains have sizes between 2 μm and 5 μm, i.e. they are larger than typical grains in the initial microstructure and approach dimensions where dislocation spacing rather than mere grain size dominate the strength level. Additional factors promoting the cyclic slip localization are high maximum Schmid factor of both parent and twin, parallel slip configuration, or high elastic anisotropy between parent and twin.

4.3. Damage initiation in copper films with log-normal grain size distribution and mean grain size of 270 nm

Cu films fabricated by sputter deposition in 8 cycles exhibit a stable UFG microstructure with a mean grain size of about 270 nm (Fig. 9). The films are weakly textured with preferable orientations between (111) and (100) ND (Fig. 9b), while the grain size distribution is very close to symmetric log-normal with virtually no grains larger than 900 nm. The fraction of TBs in these films was about 25%.

For this thin film microstructure, localized extrusions acting as damage initiation sites can be clearly detected after 3000-5000 cycles with 1% strain, as demonstrated in Fig. 10a and b. In analogy to the previous case, local plasticity occurred in large grains with equivalent diameters between 1 and 3 μm. Grains in this size range did not exist in the initial microstructure, therefore dynamic grain

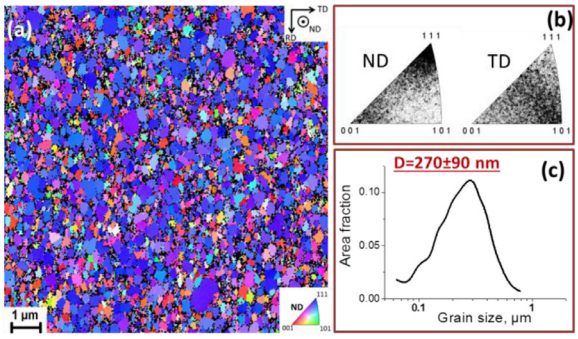

Fig. 9. Initial microstructure of 500 nm thick Cu deposited in 8 sputtering cycles. The EBSD grain orientation map is shown in (a), the corresponding inverse pole figures in (b) and the related grain size distribution in (c).

coarsening played again a significant role. In virtually all cases the extrusions were formed close to a CTB.

Detailed EBSD analysis of the microstructure surrounding the crack initiation sites is provided in Fig. 10c and d (see also supplementary Table S2). In this case it was not always possible to unambiguously assign parents and twins, since frequently CTBs were located between two inclusion-free grains of similar size. Otherwise, the correlations between the local microstructure surrounding the damage initiation sites are fairly similar to the previous case of the bimodal grain size distribution. In normal direction one member of a pair was commonly close to the (100) ND orientation and virtually no grains associated with local plasticity were oriented close to (111) ND. In the straining direction again all cases can be split between the three groups: either high maximum Schmid factor, high elastic anisotropy or parallel slip configuration. A noticeable difference to the bi-modal Cu films is that the fraction of the pairs with high elastic anisotropy is higher and the ratio of parent-twin elastic moduli was in many cases more than 2. Additionally, about 30% of damage initiation sites fulfilled two of the additional parameters (e.g. high Schmid factor and parallel slip configuration) simultaneously. We attribute this to the lower initial texture, which provides a larger pool of possible orientations within the parent-twin pairs.

4.4. Damage initiation in non-textured copper films with log-normally distributed grains and average size of about 800 nm

The 500 nm thick Cu films deposited by sputtering in one cycle without interruptions exhibit a texture-free microstructure with an average grain size of 820±240 nm and a log-normal grain size distribution (Fig. 11). The fraction of TBs is about 60%, which is significantly higher than in the previous cases. It is important to note that there is a noticeable amount of grains larger than 1 μm present in the initial microstructure (Fig. 11c).

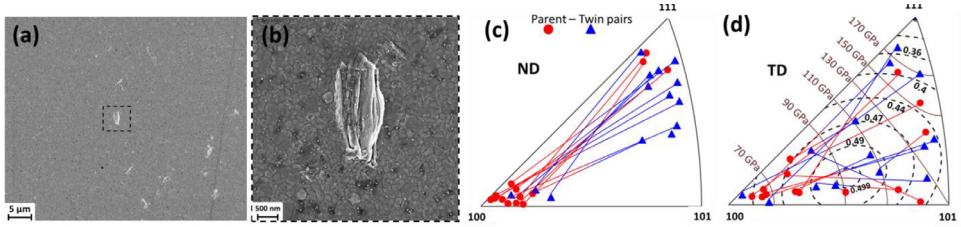

Fig. 10. Initiation of fatigue damage in 500 nm thick Cu films with log-normal grain size distribution and average grain size of 270 nm. An SEM image of typical damage initiation sites after 5000 straining cycles is shown in (a) and the corresponding enlarged view in (b). Inverse pole figures depicting the orientations of parent and twin grains in the surface normal direction and straining direction are shown in (c) and (d), respectively. Straining direction is horizontal.

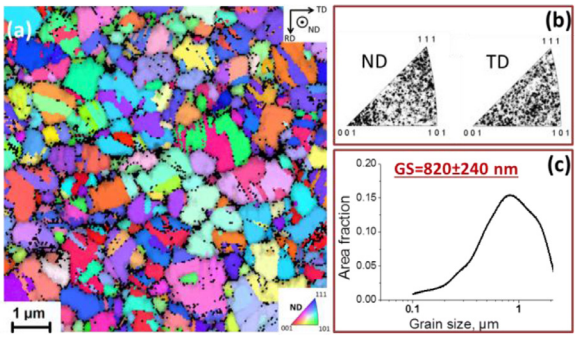

Fig. 11. Initial microstructure of 500 nm thick Cu deposited via a single sputtering cycle. The EBSD grain orientation map is shown in (a), the corresponding inverse pole figures in (b) and the related grain size distribution in (c).

Cyclic strain of 1% induced numerous local plasticity events, resulting in the formation of surface slip bands and extrusions (Fig. 12a and b) already after 1000-2000 cycles. In terms of the activation energy landscape concept (Fig. 1), this system clearly corresponds to case 3. With such a high initiation density it is rather difficult to determine which initiation site will develop to a crack and which will remain in form of localized plasticity. We consider that more pronounced extrusions, such as the one depicted by an arrow in Fig. 12b, have higher chances to initiate a crack than just a surface slip band. The analysis of parent-twin orientations (Fig. 12c and d) revealed that crack initiation sites can be again split into the three above mentioned groups (see also supplementary Table S3). In normal direction the orientation of damage initiating pairs have larger spread than in previously considered Cu films (Fig. 12c compared to Figs. 10c and 8c), and some of the extrusions are inclined with respect to the tensile axis (Fig. 12b). These trends could be clearly attributed to the absence of texture and high fraction of CTBs that greatly extends the range of parent-twin configurations with low activation energy. It is important to note that, in contrast to the cases considered above, no grain coarsening occurred in these films. To prove this convincingly, the same surface area was examined before and after cyclic straining, see supplementary Fig. S7. Even in the vicinity of local plasticity events no grain coarsening was observed. The absence of grain coarsening is attributed to high initial grain sizes with a significant fractions of grains with sizes between 1 and 2 μm.

5. Discussion

Initiation of fatigue damage in UFG films can be well understood in the frameworks of the activation energy landscape concept (Fig. 1). On the basis of presented results, one can state that the two main conditions for a deep minimum in activation energy for plastic slip localization are the existence of a CTB and a grain size of at least 1 μm. In addition to these primary conditions, at least one of the secondary conditions, i.e. high maximum Schmid factor (≥0.48) of parent or twin grain, high elastic anisotropy between parent and twin, or a parallel slip configuration, must be satisfied.

In Table 2 comparative quantitative analysis of the primary and secondary parameters for all considered film systems is presented. The gold films exhibit high texture and low amount of CTBs in the initial microstructure, thus having no deep activation energy minima. However, dynamic grain coarsening leads to appearance of large grains where dislocation slip can be activated, even without the presence of CTBs and at relatively low maximum Schmid factors. Since the amount of CTBs does not increase significantly during the grain coarsening process, the grain size remained the sole parameter responsible for the initiation of fatigue damage in this case.

Despite different initial grain sizes and textures, all considered Cu films in general obey similar selection rules for fatigue damage initiation sites. As follows from Table 2, the secondary conditions are distributed slightly differently between the initiation sites in different sample types. Some parent-twin pairs satisfy two of three secondary conditions simultaneously, leading the sum of observation frequencies to exceed 100% (see also supplementary Tables S1, S2, S3).

Notably, in both 500 nm thick Cu films the parent grains responsible for damage initiation have nearly the same size. In one case the grains coarsen substantially to reach this size (see Fig. 9c), while in the other case there was no coarsening at all. This observation indicates that there is an important transition scale of about

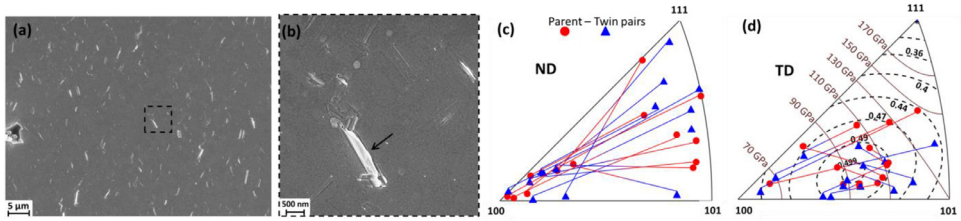

Fig. 12. Initiation of fatigue damage in 500 nm thick Cu films with log-normal grain size distribution and an average grain size of 820 nm. SEM micrograph of typical damage initiation sites after 2000 straining cycles is shown in (a) and the corresponding enlarged view in (b). Inverse pole figures depicting the orientations of parent and twin grains in the surface normal direction and straining direction are shown in (c) and (d), respectively.

Table 2
Quantitative analysis of the grains associated with fatigue damage initiation in considered thin film systems. The grain sizes are average values from at least 30 damage initiation events for each sample type. Additional factors are characterized by percentage of cases where observed. The sum of additional factor fraction values exceeds 100%, since two of three additional factors are satisfied simultaneously in some cases.

N	Material, thickness [nm]	Vicinity of TB	Average grain size [μm]	Dynamic coarsening	Secondary conditions:		
					Schmid factor ≥0.48	Elastic moduli ratio ≥1.6	parallel slip
1	Au, 250 nm	no	2.85±0.87	very strong	N/A	N/A	N/A
2	Au, 500 nm	no	2.23±0.58	very strong	N/A	N/A	N/A
3	Cu, 250 nm	yes	3.04±0.91	strong	47%	24%	42%
4	Cu 500 nm	yes	1.34±0.36	strong	39%	45%	48%
5	Cu 500 nm	yes	1.37±0.33	absent	57%	26%	51%

1 μm for the activation of cyclic plastic slip localization. In fact, no grains smaller than 900 nm were involved in damage initiation. This is most likely related to the fact that for common dislocation densities, at this length scale dislocation interaction changes from dislocation-dislocation dominated to dislocation-grain boundary related.

The average size of grains associated with damage initiation was the highest in 250 nm Cu with bi-modal initial grain size distribution. Although grain coarsening was also observed in this case, we cannot rule out that some sparsely distributed 2-3 μm large outliers were present in the initial microstructure.

The described correlations in local microstructure between the damage initiations sites in Cu films are very similar with those reported for a bulk Ni-based superalloy having rather complex precipitate-containing microstructure with an average grain size of about 30 μm by Stinville et al. [13–15]. It appears that Stinville and co-authors have provided a universal description of fatigue damage initiation mechanism for conventional grain sizes: the damage is initiated close to CTBs if either the maximum Schmid factor of the parent grain is high, or the difference in elastic stiffness between parent and twin is high, or the length of a CTB is at least two times larger than the average grain size [15]. With the results presented in the current work, it becomes clear that this mechanism spans over different materials, grain sizes and sample geometries (bulk vs. polymer-supported thin film) as long as the microstructure contains a noticeable fraction of twin boundaries and significant fraction of grains larger than 1 μm.

The impact of dynamic grain coarsening on fatigue life and material reliability is somewhat controversial. On first sight, grain coarsening seems to be detrimental for cyclic reliability, since it leads to decrease of local yield stress and accelerated plastic slip localization. However, grain coarsening through grain boundary migration is a mechanism of plasticity that itself does not lead to permanent plastic deformation. In some sense it substitutes dislocation slip, thus dissipating the excessive (non-elastic) energy without formation of slip steps. As an example, it was shown that the average grain size of thin gold film subjected to cyclic strain did grow by 300%, but no slip steps or permanent deformation was observed on the surface [40]. Grain coarsening can also help to slow down the crack propagation, especially in nanocrystalline materials that have increased strength but limited plasticity [48]. With the possibility of grain coarsening, crack propagation turns into a multi-step process involving GB migration and grain coarsening at the crack tip, succeeded by formation of slip steps, growth of extrusions and intrusions and, finally, stepwise crack extension [19]. This way, the crack must follow the differently oriented active slip planes in neighboring grains, which also leads to the extension of the crack path.

The influence of film thickness can be also evidenced from the presented results, since two films with similar microstructure but different thicknesses (both Au films) were considered. We can state that fatigue damage initiation *mechanism* does not depend considerably on film thickness. However, the kinetic parameters of damage initiation can be influenced strongly, as in the case of 500 nm thick Au films where dynamic grain coarsening and surface slip step formation were much faster with increasing cycle number in comparison to 250 nm thick films.

Bimodal microstructures are known to be beneficial for increasing ductility in nanocrystalline and UFG materials without a significant reduction in strength [49]. However, in the case of cyclic loading, rather marginal effects of bimodal microstructure on fatigue life were reported [50]. In the particular case of Cu films with bi-modal microstructure, no significant improvement of the fatigue properties was observed due to the existence of a small fraction of favorably oriented large grains with CTBs. These damage initiation sites were of low activation energy and thus responsible for all initiated cracks, while the rest of the film remained damage-free (Fig. 7).

In the current work we have considered a relatively high value of total cyclic strain amplitude ($\Delta\varepsilon$=1%), which corresponds to a low-cycle fatigue regime. It is supposed that the main conclusions can also be extrapolated to lower strain amplitudes (high-cycle fatigue) in line with the picture of the activation energy landscape concept. At lower strain amplitudes only the deepest energetic minima will be activated, which should result in a narrower parameter range of potential initiation sites. In fact, this trend was directly demonstrated in [14], where the same material was subjected to different cyclic strains. If in low-cycle fatigue regime the range of maximum Schmid factors started at 0.45, in high-cycle fatigue only grains with a maximum Schmid factor exceeding 0.495 were involved in plastic strain localization.

As a final remark, it is important to mention that within the current EBSD-based experimental approach, not all material properties relevant for fatigue damage initiation can be captured. In particular, initial defect and dislocation densities as well as the amount of dislocation sources remain unknown, and could act as hidden parameters influencing plastic slip localization. It is, however, understood that even if such hidden factors do play a substantial role in the fatigue damage initiation process, their discovery will not invalidate the presented analysis, but would rather extent it.

6. Conclusions

By employing thin films deposited on polymer substrates, the early stage of fatigue damage in UFG Au and Cu was investigated with the aim to identify how the formation of damage initiation sites is related to the local and global microstructure. It is shown that fatigue damage is initiated in the vicinity of specifically oriented CTBs which involve either a grain with a high maximum Schmid factor, parallel slip configuration, or large elastic anisotropy between parent and twin in straining direction. The local grain size is also a crucial parameter, since the grains where local plasticity was observed were over 900 nm in equivalent diameter in all cases, even though all microstructures were UFG in average. In highly textured films with a low fraction of TBs the damage initia-

tion was independent from the local grain orientations and the size of dynamically coarsened grains was the sole parameter responsible for plastic slip localization. The effect of global microstructure can be understood in terms of the activation energy landscape concept. Global parameters which provide a large pool of potential damage initiation sites are low texture, high fraction of TBs, and a high fraction of large grains with sizes exceeding 1 μm in the initial microstructure.

Provided experimental observations allow to formulate a recipe for extension of fatigue life of UFG thin films. Low amounts of TBs and strong (111) ND texture will significantly reduce the density of potential initiation sites (i.e. deep minima on activation energy landscape will be avoided). An additional important requirement is the narrow grain size distribution restricted to the low UFG range ($<$500 nm). Strategies to impede GB migration and grain coarsening by grain boundary pinning or grain boundary segregation might help to increase the number of cycles until cracks start to propagate. However, this requires some balancing, as grain coarsening is believed to help to dissipate plastic energy and to extent the fatigue life by delaying fatigue initiation.

Declaration of Competing Interest

The authors declare that they have no known competing financial interests or personal relationships that could have appeared to influence the work reported in this paper.

Acknowledgements

O.G. would like to acknowledge financial support from Austrian Science Fund (FWF) through the projects P27432-N20 and P31544-NBL. D.K. acknowledges funding by the European Research Council under Grant number 771146 (TOUGHIT) and helpful discussions on data visualization with Dr. P. Lehto.

Supplementary materials

Supplementary material associated with this article can be found, in the online version, at doi:10.1016/j.actamat.2020.116599.

References

[1] U. Essmann, U. Gösele, H. Mughrabi, A model of extrusions and intrusions in fatigued metals I. Point-defect production and the growth of extrusions, Philos. Mag. A Phys. Condens. Matter, Struct. Defects Mech. Prop. 44 (1981) 405–426, doi:10.1080/01418618108239541.
[2] K. Differt, U. Esmann, H. Mughrabi, H. Mughrabi, A model of extrusions and intrusions in fatigued metals II. Surface roughening by random irreversible slip, Philos. Mag. A Phys. Condens. Matter, Struct. Defects Mech. Prop. 54 (1986) 237–258, doi:10.1080/01418618608242897.
[3] P. Lukáš, L. Kunz, Role of persistent slip bands in fatigue, Philos. Mag. 84 (2004) 317–330, doi:10.1080/14786430310001610339.
[4] J. Man, K. Obrtlík, J. Polák, Extrusions and intrusions in fatigued metals. Part 1. State of the art and history, Philos. Mag. 89 (2009) 1295–1336, doi:10.1080/14786430902917616.
[5] M.D. Sangid, The physics of fatigue crack initiation, Int. J. Fatigue 57 (2013) 58–72, doi:10.1016/j.ijfatigue.2012.10.009.
[6] C. Blochwitz, R. Richter, Plastic strain amplitude dependent surface path of microstructurally short fatigue cracks in face-centred cubic metals, Mater. Sci. Eng. A. 267 (1999) 120–129, doi:10.1016/s0921-5093(99)00060-x.
[7] C. Blochwitz, W. Tirschler, Influence of texture on twin boundary cracks in fatigued austenitic stainless steel, Mater. Sci. Eng. A 339 (2003) 318–327, doi:10.1016/S0921-5093(02)00126-0.
[8] C. Blochwitz, S. Jacob, W. Tirschler, Grain orientation effects on the growth of short fatigue cracks in austenitic stainless steel, Mater. Sci. Eng. A 496 (2008) 59–66, doi:10.1016/j.msea.2008.04.050.
[9] M. Mineur, P. Villechaise, J. Mendez, Influence of the crystalline texture on the fatigue behavior of a 316L austenitic stainless steel, Mater. Sci. Eng. A 286 (2000) 257–268, doi:10.1016/S0921-5093(00)00804-2.
[10] R.C. Boettner, A.J. McEvily, Y.C. Liu, On the formation of fatigue cracks at twin boundaries, Philos. Mag. 10 (1964) 95–106, doi:10.1080/14786436408224210.
[11] A.I. Thompson, The influence of grain and tlin boundaries in fatigue cracking, Acta Metall. 20 (1972) 1085–1094, doi:10.1016/0001-6160(72)90172-1.
[12] A. Heinz, P. Neumann, Crack initiation during high cycle fatigue of an austenitic steel, Acta Metall. Mater. 38 (1990) 1933–1940, doi:10.1016/0956-7151(90)90305-Z.
[13] J.C. Stinville, N. Vanderesse, F. Bridier, P. Bocher, T.M. Pollock, High resolution mapping of strain localization near twin boundaries in a nickel-based superalloy, Acta Mater. 98 (2015) 29–42, doi:10.1016/j.actamat.2015.07.016.
[14] J.C. Stinville, W.C. Lenthe, J. Miao, T.M. Pollock, A combined grain scale elastic-plastic criterion for identification of fatigue crack initiation sites in a twin containing polycrystalline nickel-base superalloy, Acta Mater. 103 (2016) 461–473, doi:10.1016/j.actamat.2015.09.050.
[15] J.C. Stinville, W.C. Lenthe, M.P. Echlin, P.G. Callahan, D. Texier, T.M. Pollock, Microstructural statistics for fatigue crack initiation in polycrystalline nickel-base superalloys, Int. J. Fract. 208 (2017) 221–240, doi:10.1007/s10704-017-0241-z.
[16] G.P. Zhang, C.A. Volkert, R. Schwaiger, P. Wellner, E. Arzt, O. Kraft, Length-scale-controlled fatigue mechanisms in thin copper films, Acta Mater. 54 (2006) 3127–3139, doi:10.1016/j.actamat.2006.03.013.
[17] T. Hanlon, E.D. Tabachnikova, S. Suresh, Fatigue behavior of nanocrystalline metals and alloys, Int. J. Fatigue 27 (2005) 1147–1158, doi:10.1016/j.ijfatigue.2005.06.035.
[18] B. Moser, T. Hanlon, K.S. Kumar, S. Suresh, Cyclic strain hardening of nanocrystalline nickel, Scr. Mater. 54 (2006) 1151–1155, doi:10.1016/j.scriptamat.2005.11.054.
[19] B.L. Boyce, H.A. Padilla, Anomalous fatigue behavior and fatigue-induced grain growth in nanocrystalline nickel alloys, Metall. Mater. Trans. A Phys. Metall. Mater. Sci. 42 (2011) 1793–1804, doi:10.1007/s11661-011-0708-x.
[20] R.A. Meirom, D.H. Alsem, A.L. Romasco, T. Clark, R.G. Polcawich, J.S. Pulskamp, M. Dubey, R.O. Ritchie, C.L. Muhlstein, Fatigue-induced grain coarsening in nanocrystalline platinum films, Acta Mater. 59 (2011) 1141–1149, doi:10.1016/j.actamat.2010.10.047.
[21] M. Goto, K. Kamil, S.Z. Han, K. Euh, S.S. Kim, J. Lee, Fatigue-induced grain coarsening and crack growth behavior in ultrafine-grained copper under different loading histories, Int. J. Fatigue 51 (2013) 57–67, doi:10.1016/j.ijfatigue.2013.02.008.
[22] C.Y. Dai, G.P. Zhang, C. Yan, Size effects on tensile and fatigue behaviour of polycrystalline metal foils at the micrometer scale, Philos. Mag. 91 (2011) 932–945, doi:10.1080/14786435.2010.538017.
[23] T. Kondo, X.C. Bi, H. Hirakata, K. Minoshima, Mechanics of fatigue crack initiation in submicron-thick freestanding copper films, Int. J. Fatigue 82 (2016) 12–28, doi:10.1016/j.ijfatigue.2015.08.019.
[24] T. Kondo, H. Hirakata, K. Minoshima, Thickness effects on fatigue crack propagation in submicrometer-thick freestanding copper films, Int. J. Fatigue 103 (2017) 444–455, doi:10.1016/j.ijfatigue.2017.06.029.
[25] A. Pineau, A. Amine Benzerga, T. Pardoen, Failure of metals III: fracture and fatigue of nanostructured metallic materials, Acta Mater. 107 (2016) 508–544, doi:10.1016/j.actamat.2015.07.049.
[26] H.A. Padilla, B.L. Boyce, A review of fatigue behavior in nanocrystalline metals, Proc. Soc. Exp. Mech. Inc. 67 (2010) 5–23, doi:10.1007/s11340-009-9301-2.
[27] O. Kraft, R. Schwaiger, P. Wellner, Fatigue in thin films: lifetime and damage formation, Mater. Sci. Eng. A 319–321 (2001) 919–923, doi:10.1016/S0921-5093(01)00990-X.
[28] R. Schwaiger, G. Dehm, O. Kraft, Cyclic deformation of polycrystalline Cu films, Philos. Mag. 83 (2003) 693–710, doi:10.1080/0141861021000056690.
[29] D. Wang, C.A. Volkert, O. Kraft, Effect of length scale on fatigue life and damage formation in thin Cu films, Mater. Sci. Eng. A 493 (2008) 267–273, doi:10.1016/j.msea.2007.06.092.
[30] S. Eve, N. Huber, A. Last, O. Kraft, Fatigue behavior of thin Au and Al films on polycarbonate and polymethylmethacrylate for micro-optical components, Thin Solid Films 517 (2009) 2702–2707, doi:10.1016/j.tsf.2008.12.018.
[31] X.M. Luo, G.P. Zhang, Grain boundary instability dependent fatigue damage behavior in nanoscale gold films on flexible substrates, Mater. Sci. Eng. A 702 (2017) 81–86, doi:10.1016/j.msea.2017.07.006.
[32] G.P. Zhang, K.H. Sun, B. Zhang, J. Gong, C. Sun, Z.G. Wang, Tensile and fatigue strength of ultrathin copper films, Mater. Sci. Eng. A 484 (2008) 387–390, doi:10.1016/j.msea.2007.02.132.
[33] J.Y. Zhang, X. Zhang, G. Liu, R.H. Wang, G.J. Zhang, J. Sun, Length scale dependent yield strength and fatigue behavior of nanocrystalline Cu thin films, Mater. Sci. Eng. A 528 (2011) 7774–7780, doi:10.1016/j.msea.2011.06.083.
[34] H.Y. Wan, X.M. Luo, X. Li, W. Liu, G.P. Zhang, Nanotwin-enhanced fatigue resistance of ultrathin Ag films for flexible electronics applications, Mater. Sci. Eng. A 676 (2016) 421–426, doi:10.1016/j.msea.2016.09.010.
[35] G.D. Sim, Y. Hwangbo, H.H. Kim, S.B. Lee, J.J. Vlassak, Fatigue of polymer-supported Ag thin films, Scr. Mater. 66 (2012) 915–918, doi:10.1016/j.scriptamat.2012.02.030.
[36] G.D. Sim, Y.S. Lee, S.B. Lee, J.J. Vlassak, Effects of stretching and cycling on the fatigue behavior of polymer-supported Ag thin films, Mater. Sci. Eng. A 575 (2013) 86–93, doi:10.1016/j.msea.2013.03.043.
[37] X.J. Sun, C.C. Wang, J. Zhang, G. Liu, G.J. Zhang, X.D. Ding, G.P. Zhang, J. Sun, Thickness dependent fatigue life at microcrack nucleation for metal thin films on flexible substrates, J. Phys. D. Appl. Phys. 41 (2008), doi:10.1088/0022-3727/41/19/195404.
[38] O. Glushko, A. Klug, E.J.W.W. List-Kratochvil, M.J. Cordill, Relationship between mechanical damage and electrical degradation in polymer-supported metal films subjected to cyclic loading, Mater. Sci. Eng. A 662 (2016) 157–161, doi:10.1016/j.msea.2016.03.052.

[39] I.M. Graz, D.P.J. Cotton, S.P. Lacour, Extended cyclic uniaxial loading of stretchable gold thin-films on elastomeric substrates, Appl. Phys. Lett. 94 (2009) 071902, doi:10.1063/1.3076103.
[40] H. Mughrabi, Cyclic slip irreversibility and fatigue life: A microstructure-based analysis, Acta Mater. 61 (2013) 1197–1203, doi:10.1016/j.actamat.2012.10.029.
[41] O. Glushko, G. Dehm, Initiation and stagnation of room temperature grain coarsening in cyclically strained gold films, Acta Mater. 169 (2019) 99–108, doi:10.1016/j.actamat.2019.03.004.
[42] C.H. Hsueh, M. Yanaka, Multiple film cracking in film/substrate systems with residual stresses and unidirectional loading, J. Mater. Sci. 38 (2003) 1809–1817, doi:10.1023/A:1023200415364.
[43] O. Glushko, A. Klug, E.J.W.W. List-Kratochvil, M.J. Cordill, Monotonic and cyclic mechanical reliability of metallization lines on polymer substrates, J. Mater. Res. 32 (2017) 1760–1769, doi:10.1557/jmr.2017.121.
[44] E.O. HALL, Variation of hardness of metals with grain size, Nature 173 (1954) 948–949, doi:10.1038/173948b0.
[45] R.W. Armstrong, 60 years of hall-petch: past to present nano-scale connections, Mater. Trans. 55 (2014) 2–12, doi:10.2320/matertrans.MA201302.
[46] A. Rajabzadeh, M. Legros, N. Combe, F. Mompiou, D.A. Molodov, Evidence of grain boundary dislocation step motion associated to shear-coupled grain boundary migration, Philos. Mag. 93 (2013) 1299–1316, doi:10.1080/14786435.2012.760760.
[47] A. Rajabzadeh, F. Mompiou, S. Lartigue-Korinek, N. Combe, M. Legros, D.A. Molodov, The role of disconnections in deformation-coupled grain boundary migration, Acta Mater. 77 (2014) 223–235, doi:10.1016/j.actamat.2014.05.062.
[48] K.S. Kumar, H. Van Swygenhoven, S. Suresh, Mechanical behavior of nanocrystalline metals and alloys, Acta Mater. 51 (2003) 5743–5774, doi:10.1016/j.actamat.2003.08.032.
[49] W. Yinmin, C. Mingwei, Z. Fenghua, M. En, High tensile ductility in a nanostructured metal, Nature 419 (2002) 912, doi:10.1038/nature01133.
[50] H.W. Höppel, M. Korn, R. Lapovok, H. Mughrabi, Bimodal grain size distributions in UFG materials produced by SPD: their evolution and effect on mechanical properties, J. Phys. Conf. Ser. (2010) 240, doi:10.1088/1742-6596/240/1/012147.